FLARING ARCHES

II. *Events in the Arch System of 6/7 November, 1980*

ZDENĚK F. ŠVESTKA

Laboratory for Space Research Utrecht, SRON, The Netherlands

FRANTIŠEK FÁRNÍK

Astronomical Institute of the Czechoslovak Academy of Sciences, Ondřejov, Czechoslovakia

JUAN M. FONTENLA*

Space Science Laboratory, NASA MSFC, Huntsville, AL 35812, U.S.A.

and

SARA F. MARTIN

Solar Astronomy, CALTECH, Pasadena, CA 91125, U.S.A.

(Received 1 January, 1989; in revised form 6 May, 1989)

Abstract. We discuss first the development of the coronal arch-shaped structure of ~ 57000 km length which was born at or before 08 : 00 UT on 6 November, 1980 and became the site of 13 quasi-periodic brightenings in hard X-rays from 10 : 00 to 14 : 30 UT. The same structure became the site of a series of 17 flaring arches between 15 : 30 and 24 : 00 UT on that day. The periodicity of ~ 19 min, defined well for the quasi-periodic variations, seems to be partly retained during the occurrence of the flaring arches.

The flaring arch studied in Paper I (called SB arch) was the brightest event of this set of events. This paper presents its extended analysis and also an analysis of three other flaring arches that occurred in this configuration. All these events exhibit similar characteristics and thus demonstrate that the 'flaring arch' is a distinct solar phenomenon with specific characteristic properties.

A comparison of Hα, O v, and X-ray data for the SB arch essentially confirmed, in a quantitative way, the qualitative interpretation of the flow of emitting plasma through the arch proposed in Paper I. In particular, these data show: (1) a hot conduction front producing X-rays in the least dense plasma ahead, a decelerating more dense plasma bulk seen next in O v, and still more decelerating very dense plasma eventually visible in emission in Hα; (2) a gradient of densities from the primary towards the secondary footpoint, by factor 3 in X-rays, one order of magnitude in O v, and probably more in the densest loops emitting in Hα; (3) the secondary footpoint with hard X-ray spectrum, predominantly excited by particle streams.

1. Introduction

According to Paper I (Martin and Švestka, 1988) the 'flaring arch' in an active region is a phenomenon in which X-ray and Hα emission traverse a coronal arch from one chromospheric footpoint to another. The primary footpoint is the seat of a flare or, at least, a flare-like brightening. The secondary footpoint can be at a distance of tens to several hundred thousand kilometers. Somewhat similar events were observed in Hα by Mouradian, Martres, and Soru-Escaut (1983), in X-rays by Rust, Simnett, and Smith (1985), and in UV lines by Fontenla *et al.* (1989).

* Member of the Carrera del Investigador, CONICET, Argentina.

Solar Physics **123:** 317–341, 1989.

In Paper I, Martin and Švestka studied the two brightest events of this kind known so far, on 6 and 12 November, 1980. These events occurred in the same active region Hale No. 17255, but in two different coronal arch structures. The results of Paper I, based on observations made by HXIS on board the SMM (Van Beek *et al.*, 1980) and at Big Bear Solar Observatory, can be very briefly summarized as follows:

(1) The lengths of the two arches were estimated to be 57 000 km (the SB arch on 6 November) and 263 000 km (the L arch of 12 November).

(2) The primary footpoint was associated with a relatively strong and long-lived hard X-ray burst, but a relatively short-lived soft X-ray burst.

(3) With a delay of only seconds after the onset of the hard X-ray burst, the secondary footpoint began to brighten in Hα. The X-ray brightening at the secondary footpoint was more delayed.

(4) After the onset of the hard X-ray burst X-ray emission began to traverse the arch, with an average speed of 1070 km s^{-1} in the smaller arch and 1640 km s^{-1} in the large one.

(5) At about the same time an ejection of Hα-emitting material from the site of the primary footpoint was observed: with a mean speed of 114 km s^{-1} in the smaller arch and of 260 km s^{-1} in the large one.

(6) The maximum X-ray emission at the secondary footpoint was delayed with respect to the maximum at the secondary footpoint, by about 53 s in the smaller arch and 7.5 min in the large one.

(7) In the smaller arch, the X-ray spectrum of the maximum flux at the secondary footpoint was distinctly harder than at the primary site of the ejection.

(8) The arches consisted of sets of threads, apparently of widely different densities.

Both these major events occurred in configurations that persisted in the active region for more than one day. Many weaker events of flaring arches repeatedly appeared in these long-lived structures and also other kinds of brightenings seemed to be related to them. In this Paper II we will present the life story of the coronal structure in which the smaller (SB) flaring arch of 17 : 34 UT on 6 November occurred and we will analyze three weaker flaring arches that occurred in the same structure and followed the major SB event later on 6 November. We will also include into our analysis observations of the SB arch in the O v line of the UVSP experiment on board the SMM (Woodgate *et al.*, 1980) which were not considered in Paper I.

We do not attempt in this paper to do a similar analysis for the second, large structure in which the major flaring arch of 12 November appeared. During that time (10 to 13 November) the pointing system of the SMM started to malfunction intermittently so that there are many gaps in data and many images without stabilized pointing; as a consequence, we do not have any other flaring arch event of this series observed well both in Hα and in X-rays.

2. Time History of the Arch Structure of 6 November, 1980

2.1. Birth of the Structure

The area which later became the site of the primary footpoint of the flaring arches first became visible in X-rays at about 08 : 10 UT on 6 November (Figure 1(b)) during a major long-lived flare. It might have been present there even before that time, because the major dynamic flare (importance X9, onset 03 : 29 UT) was slowly decaying in the morning hours of 6 November and its X-ray radiation still dominated the HXIS field of view during the preceding SMM orbit (cf. Figure 1(a)). No observations of this active region were made by HXIS prior to the flare onset.

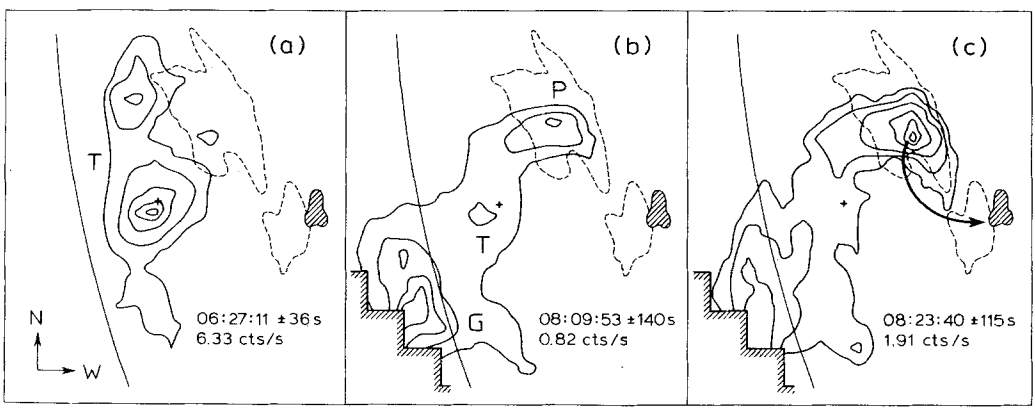

Fig. 1. 3.5–5.5 keV X-ray images of AR 17255 on 6 November, 1980 with spatial resolution of 8 arc sec in the fine field of view of the Hard X-Ray Imaging Spectrometer (HXIS). The solar limb (full curve), contours of the Hα plage (dashed lines) and the umbra of the big spot in AR 17255 (shaded patch) are indicated. The brightness contours in X-ray images follow the sequence of 90, 75, 50, 12.5, and 6.25% of the maximum count (equal to cts s^{-1} given in each frame). The tops (T) of the 'post'-flare loops of the dynamic flare that began at 03 : 29 UT are clearly seen in (a) at 06 : 27 UT. In (b), at 08 : 10 UT, only a week remnant of the loops is still visible, but two new structures appeared in the image: emission of the giant post-flare arch (G) slightly above the limb, and a new formation (P) in the plage which later became the seat of the primary footpoint of the flaring arches. This region might have been newly formed, or became visible because of decreased emission of the flare. Its growth in intensity in (c), at 08 : 24 UT, indicates that it may be a newly born structure. An arrow shows the shape of the flaring arches formed in this AR after 15 : 20 UT the same day.

2.2. Quasi-Periodic Variations

Starting at 10 : 00 UT this area became the site of a series of quasi-periodic X-ray, microwave, metric-radio, and UV brightenings described and analyzed by Švestka *et al.* (1982, 1983; cf. Figure 4 in the 1982 paper). Altogether thirteen sequential brightenings appeared, following in intervals of about 20 minutes, the last of them with its peak at 14 : 13 UT. They are summarized in Table I as events No. 1 through 13.

The first brightening in this series occurred at the site of the primary footpoint only. The existence of the secondary footpoint was first indicated by instruments on board

TABLE I

Time history of the brightenings occurring in the flaring arch structure of 6 November, 1980

Event No.	Time of HXIS[a] (3.5–5.5 keV) maxima (UT)	Times of GOES-2[b] (3.1–24 keV) maxima (UT)	Hα observations[c] of the arch structure (UT)
	Quasi-periodic variations		
1	10:12 HXR	10:12 M	Sf, one footpoint
2		10:39 M	0
3		11:06 M	Sf, one footpoint
4		11:23 M	Sf, two footpoints
5	11:46 HXR	\	Sf, two footpoints
6		11:46 M	0
7		12:05 M	0
8	≥ 12:32 HXR	12:18	0
9		12:36	0
10	13:09 HXR	12:52* M	0
11		13:13* M	0
12		13:31	0
13	14:13 HXR	13:48	0
		14:12	
	Major flare		
14	> 15:00 HXR	15:10 M	gradual arch brightening followed by a 2N/X1 dynamic flare
	Flaring arches		
			onset times:
15	/ ** 00	– **	15:28
16	/ ** 00	– **	16:19
17	/ ** 00	– ** M	16:44
18	17:23 HXR	17:20 M	17:23
19	/ HXR	– \	17:56
20	/ 00	18:14 M	18:14
21	/ 00	– M?	18:34
22	18:58 00	– \	only end seen
23	19:35 HXR	blend M	19:34
24	20:28 HXR	20:27 \	20:28 ***
25	21:09 00	– M	21:02
26		21:24 \	21:18
27	/ 00	21:40 M?	21:40
28	/ 00	– \	22:12
29	/ HXR	22:20 M	22:20
30		– \	23:02
31		23:20 \	23:20

Notes:

[a] /: no X-ray event recognizable. HXR: Hard X-ray burst (> 29 keV) recorded by the Hard X-Ray Burst Spectrometer (HXRBS; Orwig, Frost, and Dennis, 1980); 00: no hard X-ray burst reported (Dennis *et al.*, 1988). No entry: no data available.

[b] –: no X-ray event recognizable. M: a microwave burst reported (prior to 15:00 UT by Fürst and Hirth in Švestka *et al.*, 1983; by G. Hurford (private communication) after 15:00 UT). \: no microwave burst reported. No entry: no data available.

[c] 0: no Hα flare associated with the brightening.

* GOES data blended; the time is taken from microwave data.

** The decaying dynamic flare dominates the X-ray emission so that weaker events cannot be recognized.

*** Gap in Big Bear data. The time is taken from Haleakala data (courtesy M. K. McCabe).

the SMM at about 11 : 40 UT (brightening No. 5). At that time the Ultraviolet Spectrometer and Polarimeter (UVSP) showed separate brightenings in the transition-layer O v line at both the footpoints (Woodgate in Švestka *et al.*, 1982). The 3.5–5.5 keV X-ray images showed an extension towards the secondary footpoint (Figure 2(a)) and the X-ray flux near the site of the secondary footpoint reached approximately 7% of the flux at the primary site.

According to *Solar Geophysical Data* (1983), Charkov Hα patrol station reported a tiny subflare at the time of brightening No.5, with two patches apparently close to the two footpoints of the coronal arch indicated by the arrow in Figure 1(c). The flare part close to the primary (northern) footpoint brightened 3 min before the brightening near the secondary (southern) footpoint. About 20 min prior to that (at 11 : 20 UT, during the brightening No. 4 for which no SMM data was available) Charkov reported a similar subflare. This indicates that the coronal connection, which later brightened in the form of flaring arches, did exist already at that time, though no connecting arch could be seen either in UV lines or in Hα.

Charkov also reported two earlier subflares, during the first (10 : 12 UT) and third (11 : 06 UT) X-ray brightenings but then the Hα enhancement occurred only at the primary site. As we mentioned above, also in 3.5–5.5 keV X-rays the secondary footpoint did not brighten at 10 : 12 UT (no SMM data are available for 11 : 06 UT) thus being below 2% of the flux at the primary site. Hence, either the connection did not yet exist at this time, forming only later between 11 : 06 and 11 : 20 UT, or the disturbance originating at the primary site could not propagate through the existing connection prior to 11 : 20 UT.

Figures 2(a) and 2(b) show the shape of the arch structure in X-rays during two of the quasi-periodic brightenings (Nos. 5 and 8 in Table I). HXIS makes it also possible

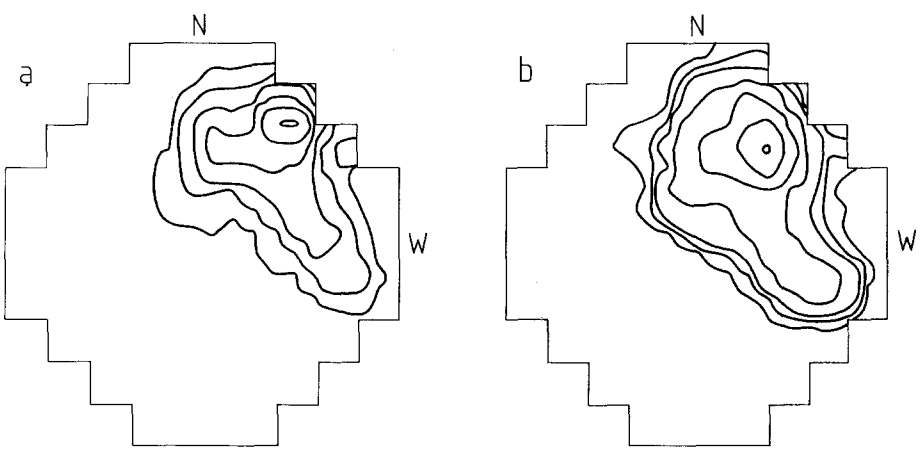

Fig. 2. X-ray images of the quasi-periodic brightenings No. 5 (a) and 8 (b) obtained in the fine field of view of the Hard X-Ray Imaging Spectrometer (HXIS) on board the SMM: (a) at 11 : 47 : 33 UT (mean time of 3 min integration of counts in the energy range 3.5–5.5 keV), max. 41.7 cts s^{-1}; (b) at 12 : 29 : 58 UT (mean time of 5 min integration of counts in the energy range 5.5–8.0 keV), max. 47.9 cts s^{-1}. The lowest contours correspond to 0.14 cts s^{-1}.

to study the time development of the X-ray flux in the individual pixels of its field of view (one pixel corresponds to 8 × 8 arc sec in HXIS fine FOV) and Figure 3 uses this capability to show the 3.5–5.5 keV flux variations at the primary and secondary footpoints of the arch during the brightening No. 5. Also included in that figure are records of the total flux in the O v line and in hard X-rays. These data reveal three sequential energy releases: the first one at 11 : 41 UT is well seen in O v and in hard X-rays, and occurs at both footpoints; the second one at 11 : 43 UT is also seen at both footpoints, and quite strongly at the secondary one, but has no response any more in

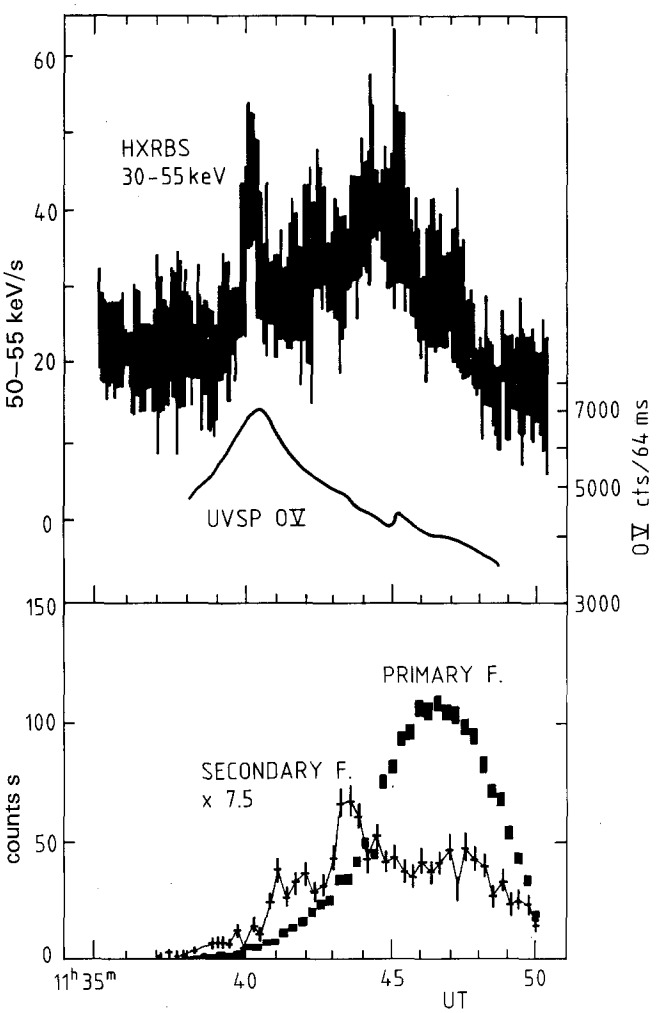

Fig. 3. *Below*: time developments of the X-ray flux in the energy range 3.5–5.5 keV at the two footpoints of the arch during the brightening No. 5 (HXIS). *Above*: time development of the total emission during this brightening in hard X-rays (Hard X-Ray Burst Spectrometer, HXRBS; Orwig, Frost, and Dennis, 1980) and in the O v line in the transition layer (Ultraviolet Spectrometer and Polarimeter, UVSP). The two upper curves have been taken from Figure 7 in Švestka *et al.* (1982).

O v; eventually the main burst, peaking at 11 : 45–11 : 46 UT, has only a weak response at the secondary footpoint, delayed by about 1 min.

O v showed the secondary footpoint only during the first energy release; a detailed comparison of microwave and metric radio records at that time (cf. Figure 6 in Švestka *et al.*, 1983) shows that this first energy release was produced by electrons streaming upwards from a site near the primary footpoint with a speed of $> 75\,000$ km s^{-1}. Thus it is likely that this first phase was a release of electrons from the primary footpoint; a part of these electrons traveled upwards into the corona producing the associated type III-like radiobursts, while another part was guided through the existing arch system to the site of the secondary footpoint. The ensuing energy releases probably originated in the corona (cf. Švestka *et al.* who speak about 'purely coronal flare-like variations') and had an impact solely at the primary footpoint.

Thereafter, however, the connection ceased to be visible: in the brightenings No. 10 (at 13 : 09 UT) and 13 (14 : 13 UT) the X-ray flux at the secondary footpoint was again below 2% of the flux at the primary site. Though the maximum X-ray flux of the quasi-periodic brightenings was increasing with their series number (compare Table III and Figure 8 in Švestka *et al.*, 1983), high-resolution Hα photographs at Ramey station did not show any further Hα subflares or related emission at the site of the secondary footpoint.

Nevertheless, the magnetic connection probably was still existent, because it appeared again very clearly shortly after that at 14 : 44 UT, when the whole arch began to brighten in the onset phase of a major flare. The loop could be seen in X-rays for 12 min only, because then the SMM spacecraft entered the Earth shadow, but during this time the flux at the secondary footpoint in 3.5–5.5 keV X-rays gradually grew to 32% of the flux at the primary site.

One can best interpret this set of observations by assuming that the magnetic connection between the two footpoints existed all the time, at least since 11 : 20 UT, but that only some of the sequential small brightenings caused excitation of the connecting loops. (Different brightenings had their primary footpoints at slightly different locations, cf. Figure 5 in Švestka *et al.*, 1982.) However, when a major flare started in the active region at 14 : 44 UT, the whole arch system responded to it with a striking enhancement.

2.3. Flaring arches

At 15 : 26 UT the growing loop system of a second major dynamic flare began to develop from a site close to the secondary footpoint of the arch structure. (This loop system was studied in detail by Švestka *et al.*, 1987.) Two minutes later, at 15 : 28 UT, the Big Bear Observatory began to observe the first of a series of 17 distinct flaring-arch events in the same structure (Table I event No. 15). In Hα the southern part of this flaring arch appears to lie under the flare loop system. Two more flaring arches were seen at 16 : 19 and 16 : 44 UT (Table I, events No. 16 and 17). No X-ray data are available for these first 3 events, because the X-ray emission of the long-lived dynamic flare of importance X1 completely dominated the whole field of view of HXIS. Thereafter the major flaring arch (SB) described in Paper I occurred and thirteen other smaller events of a similar

kind appeared in the same coronal structure before the end of the observing day at Big Bear. Four of them occurred during periods for which HXIS data are available (cf. Table I) and three of them (Nos. 22–24) were intense enough to yield useful information from X-rays. We discuss these 3 events in Section 3. HXIS observed several other flaring arches also on 7 November, but no Hα data on these events are available at Big Bear, because the telescopes were pointed to other regions on the Sun.

2.4. THE QUASI-PERIODIC OCCURRENCE

It is of interest that the average period of the quasi-periodic variations seems to be retained during the occurrence of the flaring arches on 6 November. Figure 4 shows the distribution of time intervals between the 13 successive quasi-periodic variations (Nos. 1–13 in Table I) and between 17 successive flaring arches (Nos. 15–29 in Table I). The two distributions are very similar below $\Delta t = 30$ min, peaking at an average of 18–19 min, with a tail towards longer periods; however, flaring arches also show a second peak, at about twice this value. It is thus likely that the quasi-periodicity from the morning hours of 6 November continued in the series of flaring arches after 15 : 28 UT, but some (the weakest) have been missed in the Big Bear review of the events.

Thus the quasi-periodic variations and the flaring arches observed in AR 17255 have two features common: an association with the same coronal arch structure, and similar quasi-periodicity of occurrence. Another similarity is the association of hard (> 29 keV)

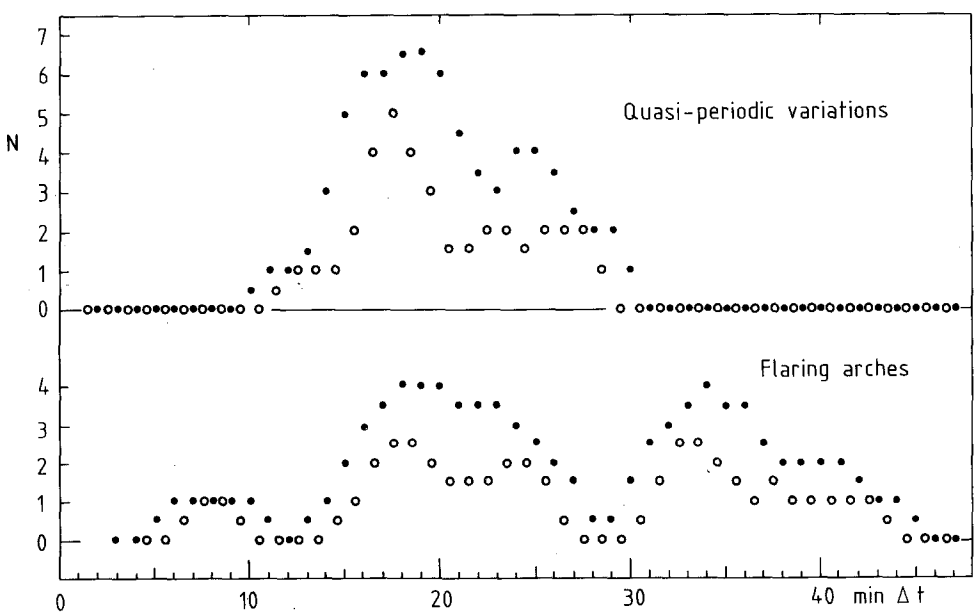

Fig. 4. Distribution of time intervals Δt between maxima of successive quasi-periodic variations (*above*) and onsets of successive flaring arches (*below*). Numbers N are smoothed values, with smoothing windows of 3 min (circles) and 6 min (dots). The real number of events was 13 for the variations and 17 for the arches.

Fig. 5. Big Bear Observatory Hα photograph of the flaring arch No. 23 in Table I, at 19:39:31 UT. We do not show Hα pictures of the other studied events: though they are clearly visible in Hα movies, it is often difficult to recognize them on a single frame.

X-rays and microwaves with relatively weak soft X-ray and Hα events. Therefore, the quasi-periodic variations observed between 10:00 and 14:13 UT seem to be the build-up to the flaring arches seen after 15:28 UT. With only one series of these events studied, one cannot understand well the relationship between these two phenomena, nor the physical reason for their quasi-periodic occurrence. Apparently, more observations of this kind are needed.

3. Other Flaring Arches in AR 17255

We will now discuss the events No. 22–24 in Table I beginning with the brightest event No. 23.

3.1. Flaring arch of 19:35 UT

The Big Bear Solar Observatory observed the onset of this event at 19:34:30 UT as a bright but very narrow mass injection from the primary footpoint into the arch structure. In contrast to the major event at 17:23 UT only few threads of the arch seemed to be affected to the extent that they became visible in emission in the Hα line. The emission reached the top of the arch at 19:39 UT (Figure 5) and the whole event was over at 19:44 UT.

The HXRBS instrument on board the SMM (Orwig, Frost, and Dennis, 1980) observed a hard X-ray burst which unfortunately was blended by a much stronger X-ray emission from another much larger flare near the center of the solar disc (Dennis, private communication). This interference did not influence the HXIS data: Figure 6 shows that the event started with a small preheating at 19:33 UT followed by a steep rise in flux at 19:35 UT. This record can be compared with the relative brightness of the Hα event photographically recorded at Big Bear Observatory. The Hα brightness at the secondary footpoint (lower part of Figure 6) began to brighten at the onset of the preheating in X-rays and another enhancement came at the time of the steep X-ray rise, at 19:35 UT. After a maximum at about 19:36 UT the Hα flux declined fast, but this

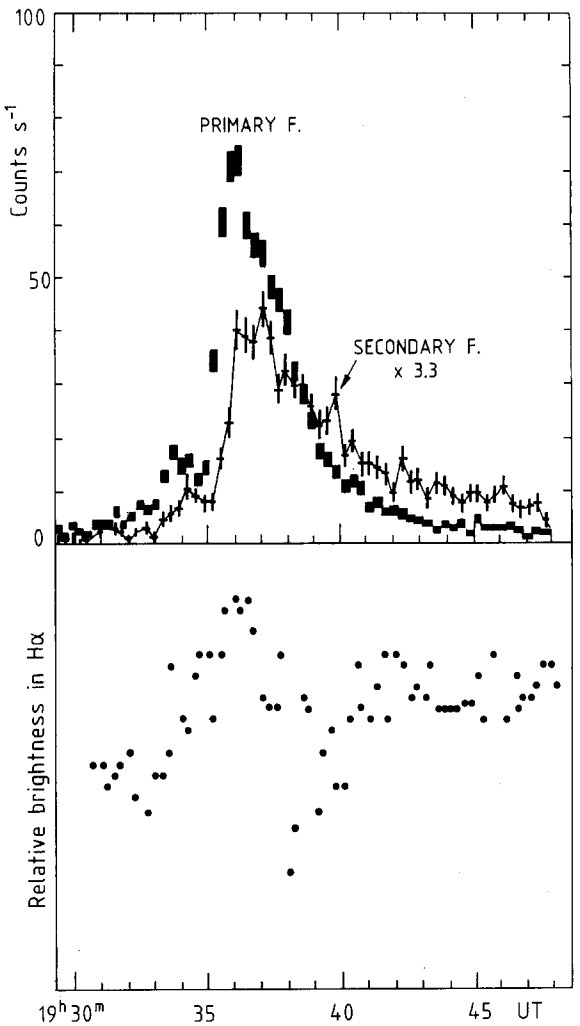

Fig. 6. *Above*: (HXIS): time development of the 3.5–5.5 keV X-ray emission at the primary and secondary footpoints of the flaring arch No. 23. *Below* (Big Bear): relative photometry of the Hα brightness at the secondary footpoint.

decline was probably due to the mass of a surge material absorbing in Hα. After less than 2 min the brightness of the secondary footpoint returned to higher level and remained at that level until the end of our measurements.

The upper part of Figure 6 compares the X-ray fluxes in the primary and secondary footpoints. Maximum flux in the energy band 3.5–5.5 keV was reached at 19 : 36 : 10 UT at the primary, and at 19 : 36 : 55 UT at the secondary footpoint. Thus the time difference between maxima was 45 s. Similar measurements in higher energy bands, 5.5–8.0 and 8.0–11.5 keV, yield 35 and 40 s, respectively (cf. Table II). Thus the average time delay was 40 s which (with the arch length of 57 000 km) corresponds to a propagation speed of 1425 km s^{-1}.

TABLE II

X-ray characteristics of three smaller flaring arches in the SB series

Event No.	22	23	24
Onset time (UT)	18 : 58	19 : 35	20 : 28
Time delay between maximum at primary and secondary footpoint			
* in band 1	35 ± 15 s	45 ± 15 s	38 ± 15 s
in band 2	35 ± 15 s	35 ± 15 s	55 ± 15 s
in band 3		40 ± 15 s	60 ± 15 s
I(secondary)/I(primary)			
* in band 1	0.39	0.18	0.21
in band 2	0.44	0.26	0.21
in band 3			0.28
* I(band 3)/I(band 1)			
at primary footpoint		0.16 ± 0.02	0.17 ± 0.02
at secondary footpoint		0.25 ± 0.04	0.19 ± 0.03
Corresponding temperature for thermal emission (after Mewe *et al.*)			
at primary footpoint		18.5×10^6 K	19.0×10^6 K
at secondary footpoint		22.0×10^6 K	19.5×10^6 K
Number of integrated pixels (7 × 7 arc sec)	3	3	6

* Band 1 = 3.5–5.5 keV; band 2 = 5.5–8.0 keV; band 3 = 8.0–11.5 keV.

Figure 7 shows X-ray images of this flaring arch at two different times in HXIS energy bands 3.5–5.5 keV and 11.5–16 keV. Only the harder images show distinctly the secondary footpoint, because at lower energies the footpoint is masked by the soft X-ray emission of the arch: the flux ratio between the secondary and the primary footpoint, and thus the relative brightness of the secondary footpoint, increases with increasing energy. This hardening of the X-ray spectrum in the secondary footpoint is demonstrated in Figure 8, where we show the time development of the (8.0–11.5 keV)/(3.5–5.5 keV) flux ratio at the two footpoints. Its value is 0.16 ± 0.02

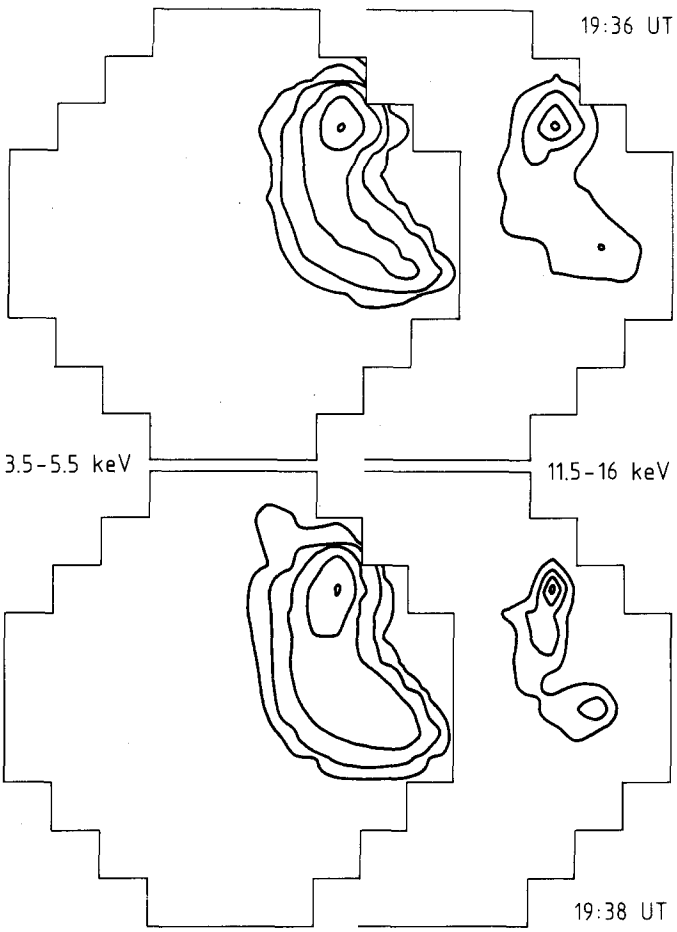

Fig. 7. X-ray images of the flaring arch No. 23. HXIS fine field-of-view, resolution 8 arc sec. *Left*: energy band 3.5–5.5 keV. *Right*: energy band 11.5–16 keV. *Above*: integration time 64 s, mean time 19 : 36 : 01 UT; contour levels: left from 28.6 to 0.31 cts s^{-1}, right 0.96 to 0.11 cts s^{-1}. *Below*: integration time 64 s, mean time 19 : 38 : 03 UT; contour levels: left from 17.4 to 0.19 cts s^{-1}, right 0.33 to 0.11 cts s^{-1}. North is up, west to the right.

at the primary footpoint and 0.25 ± 0.05 at the secondary one (sum of three pixels at each footpoint). Thus the temperature, under the assumption of thermal emission (Mewe, Gronenschild, and van de Oord, 1985), would be 22.0 million K at the secondary footpoint, and only 18.5 million K at the primary one.

All these results for the arch of 19 : 35 UT are quite similar to those obtained for the SB arch discussed in Paper I, which occurred in the same coronal configuration 2 hr and 10 min earlier: like in the SB arch, there was an X-ray precursor to the main event; the rise in X-ray flux was extremely steep; the secondary footpoint brightened in Hα at the onset of the X-ray burst at the primary site; on the other hand, the maximum of X-ray emission at the secondary footpoint was delayed with respect to the maximum at the primary footpoint and this delay corresponds to an exciting agent propagating with a

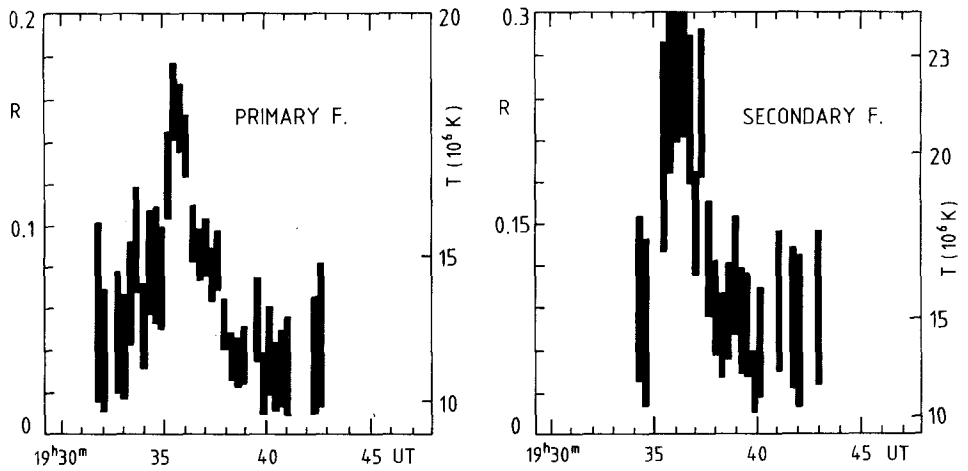

Fig. 8. Time development of the flux ratio (8.5–11 keV)/(3.5–5.5 keV) in the flaring arch No. 23. *Left*: primary footpoint; *right*: secondary footpoint. The right-hand scale gives the corresponding temperature for thermal emission after Mewe, Gronenschild, and van de Oord (1985).

speed of 1425 km s^{-1} (the corresponding speed was 1070 km s^{-1} in the SB arch); the X-ray spectrum at the secondary footpoint was harder (i.e., the fictitious temperature higher) than at the primary site, where the energy was released.

3.2. Flaring arches of 18:58 and 20:28 UT

Similar studies have been made for the arches Nos. 22 and 24 that occurred at 18:58 and 20:28 UT on 6 November, and the resulting parameters are given in Table II. Figure 9 summarizes the observed data for the arch No. 24 at 20:28 UT. One can see there the typical time delay of the X-ray emission at the secondary footpoint (Figure 9(e)) and the hardness of the X-ray spectrum at the secondary footpoint (Figures 9(f) and 9(g)). This hardness is also manifested in Figures 9(a)–9(d): the higher the imaging energy, the better is the definition of the secondary footpoint.

4. Interpretation

4.1. Hα and X-ray emission at the secondary footpoint

As discussed in Paper I, the very short delay of the Hα brightening at the secondary footpoint of a flaring arch shows that the source of the earliest brightening at the secondary site must be a flow of energetic electrons. It is quite possible that such a particle stream produces first the chromospheric Hα brightening and only later on enhancement in X-rays, because electrons lose several orders of magnitude more energy through Coulomb collisions (thus producing chromospheric heating) than through bremsstrahlung. In addition, only electrons with energy in excess of 3.5 keV contribute to the bremsstrahlung process recorded by HXIS, whereas there is no energy cutoff in the chromospheric heating. Thus some delay between the onset of emission near the

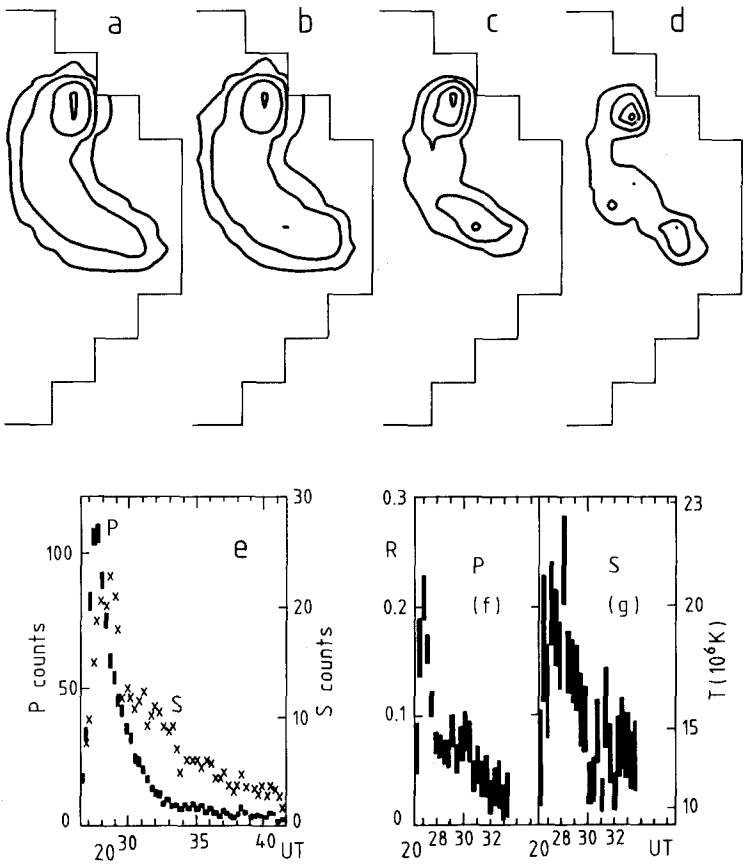

Fig. 9. The flaring arch No. 24 in Table I. (a)–(d) HXIS fine-field-of-view images at 20 : 28 : 47 ± 55 s UT: (a) 3.5–5.5 keV (max. 23.2 cts s^{-1}); (b) 5.5–8.0 keV (max. 10.5 cts s^{-1}); (c) 8.0–11.5 keV (max. 1.45 cts s^{-1}); (d) 11.5–16 keV (max. 0.36 cts s^{-1}). (e) Time development of the 3.5–5.5 keV X-ray emission at the primary (P) and secondary (S) footpoints. (f) and (g) Time development of the flux ratio (8.0–11.5 keV)/(3.5–5.5 keV) at the primary (P) and secondary (S) footpoint. The right-hand scale gives the corresponding temperature for thermal emission after Mewe, Gronenschild, and van de Oord (1985).

secondary footpoint in Hα and in X-rays is to be expected though it should be very short, because of the extremely steep rise of the primary X-ray burst.

However, if the entire X-ray flux at the secondary footpoint were due to streaming electrons, there would be no apparent reason for the observed long delay between the X-ray maxima at the primary and secondary footpoint. A 3.5 keV electron spiralling along a fieldline connecting the footpoints would need less than 4 s to traverse the arch of 57 000 km length, whereas Table II shows differences between 35 and 60 s. This difference is too large even if collisions are taken into account; besides, the effect of collisional delay should decrease with increasing energy, whereas rather the opposite is seen in Table II. Yet, as Martin and Švestka discussed in Paper I, the hardness of the X-ray spectrum at the secondary footpoint indicates that particle streams are responsible for the secondary X-ray emission, and the similarity of X-ray and Hα lightcurves

at the secondary footpoint (cf. Paper I, Figures 7 and 8) indicates that the source for both these emissions should be the same. Thus, there are three alternatives to be considered:

(A) All the X-ray and Hα emission at the secondary footpoint is caused by electrons, but their propagation is delayed by some obstacle present in the arch. This obstacle, e.g., could be a shock which propagates through the arch during the early phase and deflects a high number of particles that stream along the field lines. This hindrance in particle propagation would last until the shock reaches the secondary footpoint. The observed time delay of 35–60 s (i.e., shock speed of 1000–1900 km s^{-1}) seems acceptable.

(B) Only the earliest brightening at the secondary footpoint is caused by streaming electrons, whereas the main brightening (including the maximum flux) is caused by another slower agent. This other agent can be either:

(B1) streaming energetic protons replacing the electrons, or

(B2) a conduction front.

The case (B1) is certainly possible. Protons with energies close to 10 keV and above would fit the observed time schedule both for the arches discussed here and the L arch of Paper I. However, there is no additional evidence that would support this interpretation.

The case (B2), proposed by Rust, Simnett, and Smith (1985), could fit well the observed data (cf. Section 4.3); however, it does not explain the hardening of the X-ray spectrum near the secondary footpoint.

4.2. Hardness of X-ray spectrum near the secondary footpoint

The larger hardness of the X-ray spectrum near the secondary footpoint as compared to the primary one was demonstrated in Paper I for the SB arch and in Table II of the present paper for two other events. Martin and Švestka showed in Paper I that this hardening follows quite naturally if the secondary emission is caused by particle streams: low-energy particles suffer higher energy losses during their travel through the arch and, therefore, the resulting energy spectrum at the end point becomes harder. They also demonstrated that the observed X-ray flux and the energy spectrum at the secondary footpoint of the SB arch could be represented by power-law spectrum of the primary electrons travelling through arch threads with density of $2–4 \times 10^9$ cm^{-3}.

Let us check now other possible causes of this spectral hardening:

(i) An observational effect which might cause an apparent hardening of the X-ray spectrum at the secondary footpoint may be a concentration of the fieldlines as they extend from the primary to the secondary footpoint, thus making the secondary footpoint more compact. In this case, however, one would expect that the excess of hardness should disappear as soon as one compares more HXIS pixels near the two footpoints, which is not the case: in the SB arch, for example, in the pixel with the highest X-ray flux, the ratio $R(2/1)$ of (5.5–8.0 keV)/(3.5–5.5 keV) fluxes was 0.838 in the primary, and 0.895 in the secondary footpoint. The ratio of corresponding temperatures is thus 0.895/0.838 = 1.07. When comparing pixels with the highest ratio $R(2/1)$ one

finds temperature ratio 0.964/0.838 = 1.15. For an average of three brightest pixels the temperature ratio is 0.913/0.788 = 1.16.

We observe that the tendency is opposed to that one should expect from the effect of concentration of the fieldlines. Besides, in the X-ray images (here and in Paper I), there is no indication that such concentration of fieldlines would occur. The two footpoints seem quite comparable in size. This is also confirmed by helium D3 pictures of the SB event, made at Big Bear Observatory, which show the cores of short-lived brightenings at the two footpoints as two or three bright dots separated by about the same distance.

(ii) It is possible that while the emission at the secondary footpoint is purely non-thermal, that at the primary site has a significant thermal component. In that case the X-ray spectrum of the accelerated particles will be mixed with the much softer spectrum of thermal flare loops at the primary site, and, quite naturally, we get then harder spectrum at the secondary footpoint. This is certainly possible; a thermal flare could occur in one or a few small loops and trigger the acceleration process in another, much more extensive loop system. This is, e.g., what the Heyvaerts, Priest, and Rust (1977) flare model assumes and what Machado (1987) considers to be a general characteristic of the energy release in flares. However, a comparison of the steep rise and relative strength of the X-ray bursts related to the arches (Figures 3, 6, 9, and Paper I) indicates that the contribution of the thermal admixture during the maximum phase of the burst cannot be too large. And even in the case that its contribution causes the observed effect, *this does not remove the fact that the X-ray emission at the secondary footpoint is non-thermal, caused by streams of particles.*

Thus we do not find any way to escape the conclusion that particle streams must have been responsible, in a significant measure, for the emission of X-rays (and Hα) at the secondary footpoint. We will come back to this problem in Section 4.5.

4.3. The propagation along the arch and a conduction front

In the small arches that occurred on 6 November, details of the propagation of X-rays through the arch cannot be analyzed, because of insufficient time resolution of HXIS (cf. Paper I). However, in the L arch of Paper I, one could see quite clearly how the X-ray onset and maximum flux propagated through the arch. The alternative (B2) assumes that the gradual X-ray brightening of the arch is caused by a conduction front, and the main phase of brightening near the secondary footpoint is the final product of the front propagation. The time difference between the X-ray flux maxima at the primary and secondary footpoint then corresponds to the propagation speed of the front. This idea was proposed by Rust, Simnett, and Smith (1985) who observed several events when X-ray emission first appeared at one end of a loop and then apparently propagated along the field lines at a mean velocity between 800 and 1700 km s^{-1}. The flares discussed in Paper I were two of seven events listed by Rust, Simnett, and Smith. Their interpretation is as follows: the gradual excitation of the loops (in our case arches) is due to fast-moving thermal conduction fronts with steep temperature gradients, where fast electrons have a mean free path much larger than the scale height of the gradient.

For the speed of the heat flow they find

$$v_{cf} = 4.8 \times 10^9 \frac{T(0)^{5/2}}{n_e(0)L_T}, \tag{1}$$

where $T(0)$ is the temperature and $n_e(0)$ the electron density at the high-temperature side of the temperature gradient, and L_T is the temperature scale height.

Let us consider the brightest arch in this series, i.e., the SB arch of Paper I (No. 18 of Table I). The maximum speed of X-ray propagation in this arch (corresponding to the onset of X-ray emission at the secondary footpoint) was 1965 km s^{-1}, the mean speed (corresponding to the time difference between the maximum fluxes at the two footpoints) 1070 km s^{-1}. Apparently, the front propagates through loops of largely different densities: in other words, there must be many 'elementary conduction fronts' propagating through threads of various densities. Assuming $T(0) = 2 \times 10^7$ K (as deduced from the observed data, cf. Paper I), we thus obtain from (1)

$$n_e(0)L_T \simeq 4.4 \times 10^{19} \text{ cm}^{-2} \tag{2a}$$

in threads where the front propagates with its maximum speed, and

$$n_e(0)L_T \simeq 8.0 \times 10^{19} \text{ cm}^{-2} \tag{2b}$$

in threads where the front propagates with its mean speed.

One should mention that formula (1) was derived for a fully ionized plasma while the presence of Hα emission indicates that there is abundant neutral hydrogen in the arches. We assume that this neutral gas travels far behind the conduction front. If, however, also the material near the front is only partially ionized, this may affect to some extent the heat flow speed since this neutral material constitutes a strong sink of thermal energy and thus retards the progression of the heat flow.

We can compare Equations (2) with two kinds of data:

(1) The 'flow' of Hα emission through the arch (cf. Paper I). From the overexposed Hα images it is very difficult to determine the position of maximum intensity in the arch, but we can readily determine the times at which the leading edge of the Hα emission is seen at various distances from the primary footpoint (Table I of Paper I). The Hα emission corresponds to temperature of about 10^4 K.

(2) The 'flow' of O v emission through the loop. These data were obtained by the UVSP experiment (Woodgate *et al.*, 1980) on board the SMM and were not known to Martin and Švestka when they prepared Paper I. Figure 10 shows the time development of the O v flux in individual pixels of the UVSP raster image. Unfortunately, these data start only at 17:30:00 UT when the flaring arch was already more than 4 min in progress. Thus one does not know the onset of the O v emission, but reasonable information is received about the time of maximum O v flux at various distances from the primary footpoint. There are some secondary maxima present, the origin of which is not clear. They may either represent subsequent plasma ejections, or plasma flows along trajectories of different lengths (lower and higher in the arch: note that the radial

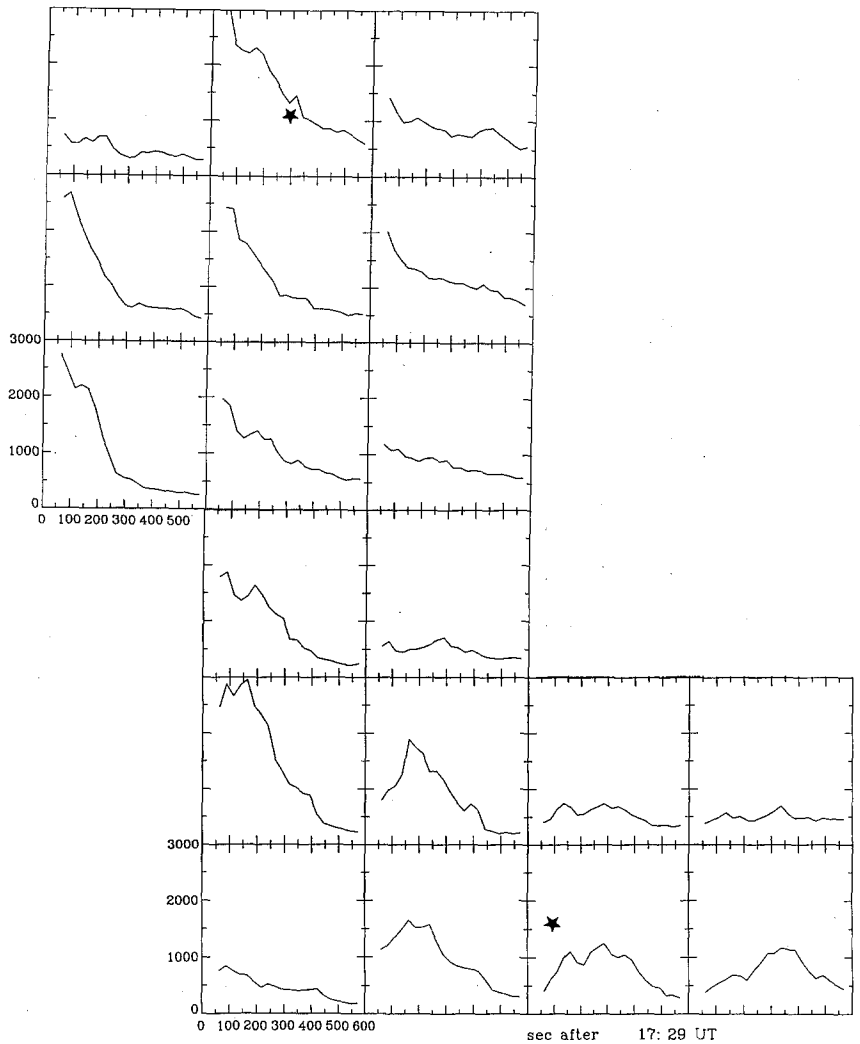

Fig. 10. Time development of the O v flux in individual pixels (10 × 10 arc sec) during the SB arch (No. 18 in Table I). The O v flux has been read by the UVSP experiment every 27 s. The vertical (counts) and horizontal (time) scales are the same for all pixels though they are shown just for two of them. Approximate positions of the two footpoints are marked by asterisks. Note that the UVSP observations started only at 17 : 30 UT, 4.5 min after the onset time of the flaring arch in Hα and X-rays. North is up and west is to the right.

extension of each pixel exceeds 7500 km and may be as large (at 65° from the central meridian) as 17 000 km). We have considered only the highest maximum in every pixel and assumed trajectories known from the Hα images. Then we get the times of O v maxima at different distances from the primary footpoint which are plotted in Figure 11 and compared to positions of the leading edge of the Hα emission. The optimum temperature for production of O v emission is 2.8×10^5 K.

Under the assumption that a conduction front is responsible for the gradual heating

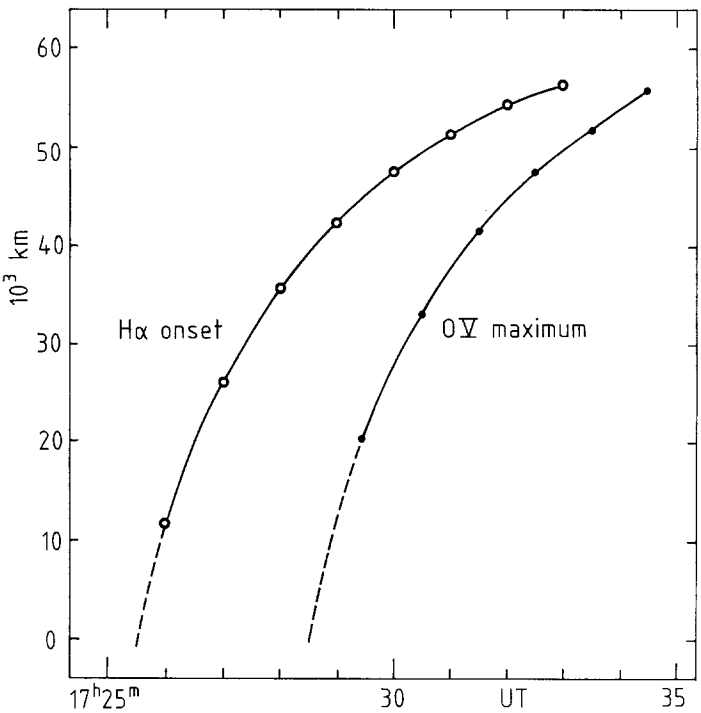

Fig. 11. Time of the Hα emission onset (i.e., position of the Hα leading edge, circles) and O v flux maximum (dots) at various distances from the primary footpoint of the SB arch (No. 18 in Table I). The Hα values have been taken from Table I of Paper I. The O v times are smoothed values based on the time of the highest maxima in Figure 10.

of the arch and that the X-ray propagation speed is a straightforward response to this heating, we can now estimate the characteristics of the front by comparing the X-rays with Hα and O v.

4.4. Cooling of the injected plasma

Let us first suppose that all the plasma injected into the arch moves with the velocity deduced from X-rays. Then the time difference between X-ray and Hα onset, or X-ray and O v maximum at a given point in the arch is simply due to the plasma cooling. We will apply here the simple method proposed by Švestka (1987) for a computation of the cooling of coronal flare loops by radiation and conduction. Under the assumption that the temperature gradient, ∇T, can be identified with the temperature scale height in Equation (1), $\nabla T = T/L_T$, the total cooling time from the initial temperature $T(0)$ to temperature $T(\tau)$, at which Hα or O v become visible is then

$$\tau = \int_{T(\tau)}^{T(0)} \frac{T^{1/2}\,\mathrm{d}T}{a + bT^4} \tag{3}$$

with

$$a = 2.9 \times 10^{-4} n_e \tag{3a}$$

and

$$b = 2.7 \times 10^{9} n_e^{-1} (L/2)^{-1} L_T^{-1}, \tag{3b}$$

where L is the length of the arch, $L = 5.7 \times 10^9$ cm, and $n_e L_T$ is given by (2a) or (2b), respectively.

In the Hα line we see the threads of the highest density, because n_e must exceed 5×10^{11} cm^{-3} to give rise to Hα emission in projection on the solar disc (Švestka *et al.*, 1987; Heinzel and Karlický, 1987). Thus from a comparison of Hα and X-ray onsets we get characteristics of the conduction fronts propagating through the densiest loops.

Taking $T(0) = 2 \times 10^7$ K and the value of $n_e L_T$ from (2a), we get $b = 2.17 \times 10^{-20}$ from (3b). Thus we can solve (3) for n_e, knowing the time delays Δt between the X-ray onset and the leading edge of the Hα emission, equal to the cooling time τ.

Δt near the primary footpoint was < 20 s. According to (3) and (2a) this requires

$$n_e > 6.6 \times 10^{12} \text{ cm}^{-3}, \qquad L_T < 66 \text{ km}; \tag{4a}$$

Δt near the top of the arch was $\simeq 100$ s, which requires

$$n_e \simeq 7.6 \times 10^{11} \text{ cm}^{-3}, \qquad L_T \simeq 580 \text{ km}; \tag{4b}$$

Δt at the secondary footpoint was 412 s, which requires

$$n_e = 8.3 \times 10^{10} \text{ cm}^{-3}, \qquad L_T = 5260 \text{ km}. \tag{4c}$$

The density values (4a) and (4b) are acceptable but the last value (4c) is obviously too low to make the loop visible in Hα emission. The density must be higher, i.e., the cooling time shorter than Δt. As one needs at least $n_e = 5 \times 10^{11}$ cm^{-3} to produce Hα emission, the cooling time, after (3) and (2a), cannot be longer than 131 s. This implies that the observed time delay Δt of 6 min 52 s at the secondary footpoint reflects the real delay of the arrival of the Hα-emitting plasma into the secondary footpoint. Thus *the plasma flowing through the densest loops clearly decelerates* from speeds in excess of > 300 km s^{-1} to < 30 km s^{-1} near the end of its flow (cf. Table I in Paper I).

The maxima of O V emission characterize less dense loops that may be close to the most common density in the arch. In the same way as before, but with $n_e L_T$ from (2b) for the mean speed (i.e., the time delays Δt between X-ray and O V maxima), we find the following characteristics for the conduction front:

near the primary footpoint:

$$\Delta t = 110 \text{ s}, \qquad n_e = 1.0 \times 10^{12} \text{ cm}^{-3}, \qquad L_T = 800 \text{ km}; \tag{5a}$$

near the top of the arch:

$$\Delta t = 230 \text{ s}, \qquad n_e = 3.6 \times 10^{11} \text{ cm}^{-3}, \qquad L_T = 2220 \text{ km}; \tag{5b}$$

at the secondary footpoint:

$$\Delta t = 480 \text{ s}, \qquad n_e = 1.1 \times 10^{11} \text{ cm}^{-3}, \qquad L_T = 7270 \text{ km}. \tag{5c}$$

If these values characterize the average (i.e., most common) conditions in the arch, the densities in (5a, b, c) should be comparable to those we have deduced from the X-ray emission in Paper I. This comparison is made in Table III. We give there, in the first line, the n_e values from (5a, b, c); in the second line, the n_e values deduced from the X-ray flux for a homogeneous X-ray emitting region with a line-of-sight extension $h = 10000$ km; in the third line then the filling factor q that would correspond to an inhomogeneous layer of $h = 10000$ km for the n_e values (5a, b, c).

TABLE III

Comparison of (5a, b, c) with parameters deduced from the X-ray emission for the SB flaring arch (event 17 in Table II)

	Primary footpoint	Top of the arch	Secondary footpoint
n_e cm^{-3} from O v	1.0×10^{12}	3.6×10^{11}	1.1×10^{11}
n_e cm^{-3} from X-rays for $h = 10000$ km and $q = 1.0$	1.2×10^{11}	3.9×10^{10}	3.7×10^{10}
q for $h = 10000$ km from O v	0.014	0.012	0.12

As mentioned in Paper I, one should be careful when considering the values deduced for the top of the arch, because there the arch might have been broader ('banana-shaped') so that the h and q parameters cannot be directly compared with those for the footpoints. Thus we will base our conclusions mainly on the data for the two footpoints in Table III. Obviously, the densities (5a, c) fit the observed X-ray fluxes for $q \simeq 0.01$ at the primary and $q \simeq 0.1$ at the secondary footpoint of the arch. These q values appear too small if we suppose that the O v data represent the most common conditions in the arch. Thus the densities in (5) are too high as compared with the observed data, in particular at the primary footpoint (and near the top).

This discrepancy will be still larger if the cooler plasma moves slower than the conduction front, as has been indicated by (4a, b, c) for the Hα data before. Thus one has to suppose (as Martin and Švestka did in Paper I) that *the bulk of the ejected plasma, which is later seen after cooling in* O v *and* Hα, *is since the ejection onset at lower temperature than the front of the ejection.* HXIS cannot image any plasma with $T < 5 \times 10^6$ K. Thus plasma below this temperature will not contribute to the X-ray emission and its density will not influence the n_e value deduced from X-rays. Thus the second line of Table III (and Table III of Paper I) yield lower density corresponding to the *extremely hot region immediately behind the conduction front which precedes a more dense, but cooler, bulk of the ejected plasma.*

4.5 TIME DELAY AT THE SECONDARY FOOTPOINT

Table III shows that the discrepancy between the densities computed in (5a) and (5c) and those deduced from X-rays is significantly larger at the primary than at the secondary footpoint. This might indicate that the inhomogeneity of the arch, very pronounced at the primary footpoint, becomes less pronounced (the inhomogeneities are 'smoothed') after the passage through the arch. This would provide some support for the interpretation (i) of the spectral hardening proposed in Section 4.2; however, as we discussed there, neither the count ratios in different HXIS pixels nor the topology of the arches indicate that the secondary footpoint becomes more compact.

Thus an alternate interpretation seems more likely: as in (4c), also in (5c) the density is underestimated, because the time delay at the secondary footpoint is not determined by cooling, but by the late arrival of the O V-emitting plasma. Thus *not only plasma in the densiest loops, but also the bulk of less dense plasma seen in the* O V *line, decelerates during its propagation through the arch.* As one can see from Figure 11, the time difference between the leading edge of the Hα emission and the maximum flux in the O V line decreases with time. Apparently, the plasma we eventually see in Hα decelerates more and faster than the plasma that we see in O V. In other words, *the largest deceleration occurs in the densest loops.*

All this does not solve the problem of the spectral hardening at the secondary footpoint. It seems that even if conduction front is a likely candidate for the propagating X-ray enhancement in the arch, the enhancement at the secondary footpoint still requires a strong admixture of thick-target bremsstrahlung from particles streaming through the arch.

We have mentioned in interpretation (A) in Section 4.1 the possibility that in the initial phase of the arch development a shock, formed by the mass ejection, may hinder the propagation of accelerated electrons from the primary towards the secondary footpoint. As Rust, Simnett, and Smith (1985) have shown, one can expect that a shock moves generally slower than the conduction front, but the eventual arrival of the thermal front and the shock at the secondary footpoint will not differ much in time. Only when the shock finishes its passage through the arch, the access of energetic particles to the secondary footpoint becomes fully opened.

This could explain the delay of the X-ray onset and maxima in the SB-type arches we study here, because enough particles were produced still at the primary site after the path had become free. It could not explain the secondary emission in the L arch of Paper I, which peaked long after the production of accelerated particles at the primary site was over; but there was no evidence that in that arch the X-ray spectrum at the secondary footpoint was harder so that particle streams need not necessarily be the prevalent source of the brightening.

Therefore, one can eventually suppose that the X-ray emission at the secondary footpoint of a flaring arch is due to a combination of conduction front heating and thick-target particle emission, of which the particle source prevails in small arches of the SB type, while the effect of the conduction front prevails in very long arches of the L type of Paper I.

5. Summary

The two major events of flaring arches discussed in Paper I (on 6 and 12 November, 1980) occurred in configurations that persisted in the active region for several days. Many weaker events, some very similar to the major arches and others with different characteristics, appeared repeatedly in these two structures. In this paper we have described and analyzed the activity that was associated with the arch structure of 6 November (which produced the SB arch of Paper I).

The area that can be identified with the primary footpoint of the flaring arches on 6 and 7 November became first visible in X-rays at about 08 : 00 UT on 6 November (Figure 1). Since 10 : 00 UT this site was the source of thirteen quasi-periodic brightenings described and analyzed by Švestka *et al.* (1982, 1983). Though this emission was confined to the primary footpoint, the existence of an arch-like connection and its secondary footpoint began to be indicated after 11 : 20 UT (Figures 2 and 3). At 14 : 44 UT, the full arch gradually began to brighten in X-rays during the onset phase of a major dynamic flare.

During the decay of this flare the first flaring arch was observed in Hα at the Big Bear Solar Observatory. Seventeen such events were recognized before midnight UT (Table I) and several more on 7 November. The quasi-periodicity of about 19 min, well defined during the occurrence of the quasi-periodic variations, seems to be partly retained in the occurrence of the flaring arches as well (Figure 4).

In addition to the SB arch of Paper I we have also analyzed three other events of this series of flaring arches, for which we have good HXIS data in X-rays (Figures 7 and 9, Hα example in Figure 5). All these events exhibit characteristics quite similar to those found earlier for the bright SB arch; in particular (Figures 6, 8, and 9, and Table II): typical steep X-ray bursts, fast enhancement of the secondary footpoint in Hα and delayed brightening in X-rays, a harder X-ray spectrum at the secondary footpoint, and delayed 'flow' of Hα emission through the arch. Thus observations of these other events demonstrate that the 'flaring arch' is a distinct solar phenomenon with specific characteristic properties.

We have then compared for the brightest SB arch the Hα data from Big Bear, O V data from UVSP, and X-ray data from HXIS, in an effort to get more information about physical characteristics of the flaring arches. Under the assumption (taken from Rust, Simnett, and Smith, 1985) that the X-ray emission, moving through the arch, is excited by a conduction front, we have obtained the following results:

An instability at the primary footpoint of the arch, marked by the steeply rising hard X-ray burst, first accelerates electrons which propagate through the least dense components of the arch system (density of the order of 10^9 cm^{-3}) and excite Hα emission at the secondary footpoint. At about the same time plasma is injected into the arch system giving rise to more and less dense arch components.

The head of the ejection creates a thermal front which gives rise to the observed X-ray emission. It propagates (in various arch-threads) with a top speed of about 2000 km s^{-1} and mean speed of $\sim$ 1000 km s^{-1}. Immediately behind the front, the plasma tempera-

ture is close to 2×10^7 K and the density decreases from about 10^{11} cm^{-3} at the primary, to $\sim 3 \times 10^{10}$ cm^{-3} at the secondary footpoint as the temperature scale height of the propagating front increases.

The bulk of the ejected plasma moves farther behind the front, with lower temperature, higher density (about 10^{12} cm^{-3} at the primary, and $\sim 10^{11}$ cm^{-3} at the secondary footpoint), and slower speed that decreases from > 600 km s^{-1} near the primary, to about 80 km s^{-1} near the secondary footpoint. This bulk of the arch plasma is visible in the UVSP O v line emission which puts a lower limit on its temperature, 3×10^5 K.

Lagging still further behind is the plasma flow in the densest threads of the arch system which eventually become visible in emission in the Hα line: the speed decreases from > 300 km s^{-1} near the primary, to ≤ 30 km s^{-1} near the secondary footpoint. The density of this rear part of the ejection must be at least 5×10^{11} cm^{-3} at the secondary footpoint (in order to appear in emission in Hα), and $> 7 \times 10^{12}$ cm^{-3} near the site of the ejection.

The ejection at the primary footpoint also gives rise to shocks which hinder the free propagation of accelerated particles through the arch. Only after the shock arrival at the secondary footpoint the particle flow can be fully restored in the arch-threads of the lowest density (cf. Paper I). The time of the shock arrival should not differ much from the arrival of the conduction front. Therefore, during the first 30–60 s (in the SB-type arches) only the Hα excitation is seen at the secondary footpoint. Strong enough bremsstrahlung (much less efficient than Coulomb collisions) must wait for the full stream of electrons after the arrival of the shock front. This flux then causes the observed hardening of the X-ray spectrum at the secondary site.

These results essentially confirm, in a more quantitative way, the qualitative conclusions made in Paper I. The results also confirm, in principle, the earlier conclusion by Rust, Simnett, and Smith (1985) that a conduction front and electron beams are two most likely mechanisms that heat solar plasma in flaring arches and similar coronal structures. (Apparently, not all events discussed by Rust, Simnett, and Smith, were flaring arches.) We have been able, by comparing soft and hard X-rays, Hα, and O v data, to make additional inferences which Rust, Simnett, and Smith, who used only soft X-ray images, could not make. It is necessary to add, however, that Alfvén wave modes and associated shocks (cf. e.g., Wu, 1987, 1988), as well as proton beams, not discussed so far in any detail, remain additional possibilities for the energy transport in flaring arches.

Acknowledgements

Radio data have been analyzed and kindly provided to us by Dr Gordon Hurford at Caltech. From Dr Marie McCabe we have got Hα data obtained at Haleakala which could supplement and confirm data from Big Bear, and from Dr B. Dennis unpublished information about hard X-ray bursts. Comments by Dr Aert Shadee on the first draft of the manuscript and by an unknown referee helped to improve the presentation. We are greatly obliged to them all.

This paper was completed when J. Fontenla held a NRCC-NAS Research Associateship. F. Fárník acknowledges financial support from SRON in The Netherlands and Z. Švestka from MSFC at Huntsville, Alabama. The contribution of S. F. Martin to this paper was supported by the Office of Naval Research under Grant N00014–82–K–0139. F. Fárník also thanks the staff on the SRON Laboratory for Space Research for valuable help during his stay in Utrecht. Thanks are due to Hans Braun in Utrecht for drawing most of the figures.

The development and construction of the HXIS was made possible by support from the Netherlands Ministry for Education and Science, and the Science and Engineering Research Council of the United Kingdom.

References

Dennis, B. R., Orwig, L. E., Kiplinger, A. L., Schwartz, R. A., Gibson, B. R., Kennard, G. S., Tolbert, A. K., Biesecker, D. A., Labow, G. J., and Shaver, A.: 1988, NASA Technical Memoradum 4036, p. 41.

Fontenla, J. M., Tandberg-Hanssen, E., Reichmann, E. J., and Filipowski, S.: 1989, *Astrophys. J.* **344**, 1034.

Heinzel, P. and Karlický, M.: 1987, *Solar Phys.* **110**, 343.

Heyvaerts, J., Priest, E. R., and Rust, D. M.:1977, *Astrophys. J.* **216**, 123.

Machado, M. E.: 1987, *Solar Phys.* **113**, 87 (and references therein).

Martin, S. F. and Švestka, Z.: 1988, *Solar Phys.* **116**, 91 (Paper I).

Mewe, R., Gronenschild, E. H. B. M., and van de Oord, G. H. J.: 1985, *Astron. Astrophys. Suppl.* **62**, 197.

Mouradian, Z., Martres, M. J., and Soru-Escaut, I.: 1983, *Solar Phys.* **87**, 309.

Orwig, L. E., Frost, K. J., and Dennis, B. R.: 1980, *Solar Phys.* **65**, 25.

Rust, D. M., Simnett, G. M., and Smith, D. F.: 1985, *Astrophys. J.* **288**, 401.

Solar Geophysical Data: 1983, No. 467, Part II, p. 34.

Švestka, Z.: 1984, *Solar Phys.* **94**, 171.

Švestka, Z.: 1987, *Solar Phys.* **108**, 411.

Švestka, Z., Dennis, B. R., Pick, M., Raoult, A., Rapley, C. G., Stewart, R. T., and Woodgate, B. E.: 1982, *Solar Phys.* **80**, 143.

Švestka, Z., Schrijver, J., Somov, B., Dennis, B. R., Woodgate, B. E., Fürst, E., Hirth, W., Klein, L., and Raoult, A.: 1983, *Solar Phys.* **85**, 313.

Švestka, Z., Fontenla, J. M., Machado, M. E., Martin, S. F., Neidig, S. F., and Poletto, G.: 1987, *Solar Phys.* **108**, 237.

Van Beek, H. F., Hoyng, P., Lafleur, B., and Simnett, G. M.: 1980, *Solar Phys.* **65**, 39.

Woodgate, B. E., Tandberg-Hanssen, E. A., Bruner, E. C., and 11 co-authors: 1980, *Solar Phys.* **65**, 73.

Wu, C. C.: 1987, *Geophys. Res. Letters* **14**, 668.

Wu, C. C.: 1988, *J. Geophys. Res.* **93**, 987.